

An AI System for Continuous Knee Osteoarthritis Severity Grading Using Self-Supervised Anomaly Detection with Limited Data

Niamh Belton^{1,2} Aonghus Lawlor^{3,4} Kathleen M. Curran^{1,2,4}

¹Science Foundation Ireland Centre for Research Training in Machine Learning

²School of Medicine, ³School of Computer Science, University College Dublin

⁴Insight Centre for Data Analytics, University College Dublin, Dublin, Ireland

Abstract. The diagnostic accuracy and subjectivity of existing Knee Osteoarthritis (OA) ordinal grading systems has been a subject of ongoing debate and concern. Existing automated solutions are trained to emulate these imperfect systems, whilst also being reliant on large annotated databases for fully-supervised training. This work proposes a three stage approach for automated continuous grading of knee OA that is built upon the principles of Anomaly Detection (AD); learning a robust representation of healthy knee X-rays and grading disease severity based on its distance to the centre of normality. In the first stage, SS-FewSOME is proposed, a self-supervised AD technique that learns the ‘normal’ representation, requiring only examples of healthy subjects and < 3% of the labels that existing methods require. In the second stage, this model is used to pseudo label a subset of unlabelled data as ‘normal’ or ‘anomalous’, followed by denoising of pseudo labels with CLIP. The final stage involves retraining on labelled and pseudo labelled data using the proposed Dual Centre Representation Learning (DCRL) which learns the centres of two representation spaces; normal and anomalous. Disease severity is then graded based on the distance to the learned centres. The proposed methodology outperforms existing techniques by margins of up to 24% in terms of OA detection and the disease severity scores correlate with the Kellgren-Lawrence grading system at the same level as human expert performance. Code available at https://github.com/niamhbelton/SS-FewSOME_Disease_Severity_Knee_Osteoarthritis.

Keywords: Few Shot Anomaly Detection · Knee Osteoarthritis · Self-Supervision · Self-Supervised Learning · X-ray · Contrastive Learning · Few Labels · CLIP · Deep Learning · Machine Learning · Artificial Intelligence.

1 Introduction

Knee Osteoarthritis (OA) is a degenerative joint disease that affects over 250 million of the world’s population [35]. Two of the most common grading systems for OA diagnosis are the Kellgren-Lawrence (KL) system [20] and the Osteoarthritis Research Society International (OARSI) atlas criteria [2,3]. The KL system consists of five ordinal classes from grade zero to four where grade zero is healthy,

grade four is severe OA and grades ≥ 2 are the cut-off for OA diagnosis [14]. The OARSI atlas criteria diagnoses OA if the subject meets specific criteria relating to the degree of Joint Space Narrowing (JSN) and the severity of osteophytes [15]. The subjectivity of these scales have been a matter of on-going concern [1] with studies reporting wide ranges of inter-observer reliability of 0.51 to 0.89 [37] for the KL system. Low agreement between the two scales has also been reported with OA being diagnosed almost twice as often using the OARSI atlas criteria compared with the KL system [14]. The variability of OA severity grading has been attributed to the difference in the level of clinician’s experience and/or the use of subjective language such as ‘possible’ osteophytic lipping and ‘doubtful’ joint space narrowing in the guidelines for grading [13]. The challenges of the current OA grading systems suggests that ordinal classes may not be suitable for assessing OA severity and highlights the requirement for an automated system.

This work aims to overcome the weaknesses of current AI systems and models for OA grading. Firstly, the high performance of existing techniques (accuracies $\geq 90\%$) is a cause for concern given the inter-rater observer reliability between human experts can be as low as 0.51 [37], suggesting that the methods have overfit to the dataset. Secondly, several of the approaches train the model as a multi-class classification problem which do not consider the ordinal nature of the data. Thirdly, existing solutions are reliant on large datasets consisting of thousands of X-rays for training, along with ground truth OA severity labels from experts which is a tedious and costly process.

This work proposes a three stage approach to designing a continuous automated disease severity system. The principle that underpins the proposed methodology is that healthy knee X-rays can be more easily identified but classifying the degree of OA severity is a subjective process. The first stage therefore, focuses solely on learning a robust representation of healthy X-rays through Self-Supervised Learning (SSL). The model FewSOME [7] is leveraged for this as it requires as few as 30 labels to achieve optimal performance and therefore, the challenge of acquiring a large dataset is eliminated. This work extends FewSOME to use SSL, namely SS-FewSOME. The OA severity of an X-ray is then assessed based on its distance in Representation Space (RS) to the centre of the normal RS, borrowing the core concept of several Anomaly Detection (AD) techniques. The second stage involves using the trained technique to pseudo label unlabelled data and denoising these labels with the CLIP model. The third stage is Dual Centre Representation Learning (DCRL), where the model contrastively learns two representations, normal and anomalous. Disease severity is then graded based on the distance to the learned centres.

The contributions of this work are;

- A newly proposed continuous OA grading system based on the principles of AD that is not trained to overfit to a subjectively graded dataset, thus removing any subjective bias.
- We advance the original FewSOME by including SSL, patch based contrastive learning, denoising of pseudo labels with CLIP and DCRL, increas-

ing the AUC for OA detection from 58.3% (original FewSOME implementation) to 72.9%.

- The proposed three stage method outperforms the existing SOTA on the task of OA detection by 24.3% (from 56.7% to 81.0%).
- This performance is achieved using a fraction of the data and less than 3% of the labels that existing methods require, eliminating the need for extensive computational resources, large annotated datasets and access to expert annotators. Thus, removing the barriers for clinical implementation and improving health equity.

2 Related Work

2.1 Automated Knee OA Severity Classification

Several fully-supervised Convolutional Neural Network (CNN) based approaches have been proposed to classify knee X-rays according to the KL system. Antony et al. [4] developed a technique to localise the knee joint area on the X-ray and then classify the OA severity using a CNN. The CNN simultaneously minimised a categorical cross-entropy loss and a regression mean squared error loss. Several works approved upon this performance by employing ensembles of CNNs [5] and implementing more advanced CNNs such as the ResNET [27], the HR-Net [18], Siamese networks [34], Long Short-Term Memory models (LSTM) [36] and dual channel autoencoders [17]. These methods were further improved by incorporating complex data pre-processing such as image enhancement [25] and noise-reduction with Gaussian-filters, normalising with a pixel-centering method, and implementing a balanced contrast enhancement technique [32]. The majority of existing techniques optimised their performance using loss functions suitable for multi-class classification, where the distance between all grades are equidistant i.e. the distance between grade zero and grade four is equal to the distance between grade zero and grade one. Culvenor et al. [13], instead, employed an ordinal loss function to take into account the ordinal nature of KL grading system. More recently, MediAI-OA [38] has advanced beyond simple KL grade classification by automatically quantifying the degree of JSN in the medial and lateral tibiofemoral joint and detecting osteophytes in the medial distal femur, lateral distal femur, medial proximal tibia and lateral proximal tibia regions.

A prior work investigated the feasibility of a continuous OA system based on Siamese networks, reporting a positive correlation between the KL grading system and the model output [24]. However, despite this progress, the existing solutions are trained to mimic a flawed grading system and they are reliant on large annotated training sets with the MediAI-OA system training on 44,193 labelled radiographs.

2.2 Anomaly Detection

AD is a field of study that aims to automatically identify data samples that differ substantially from normality. These typically involve one-class methods

such as DeepSVDD [30] and PatchCore [29] that learn or extract the features of normality and detect anomalies based on their distance to the normal RS. Generative models are another class of AD models [39], particularly popular in the medical field [11,6,40]. At training time, they learn to reconstruct the image. At test time, they can then identify anomalies by large reconstruction errors. However, SSL based methods such as Cutpaste [23] have been dominating the field of AD in recent years, with several works leveraging SSL for medical AD tasks [10,11]. Although the majority of AD techniques train on unlabelled data, a recent technique Dual-distribution discrepancy with self-supervised refinement (DDAD) [11] trains on both labelled and unlabelled data. They train an ensemble of reconstruction networks with the objective of modelling the normative distribution and a second ensemble of networks to model the unknown distribution. They then calculate the intra-discrepancy and inter-discrepancy of the distributions to assign anomaly scores. Finally they train a separate network via self-supervised learning to further refine the anomaly scores. They demonstrated their AD performance on chest X-rays and brain MRI.

There has been recent interest in Few Shot AD for settings where there is limited data. Few Shot AD focuses on learning to detect anomalies having trained on zero shots or few shots of the normal class [19,7]. FewSOME [7] is a recent few shot AD technique originally developed for poor quality data detection in medical imaging datasets [9] and has since proven its performance for AD in natural images, industrial defect detection and motion artefact detection in brain MRI [8]. FewSOME is in the category of one-class AD models as it contrastively learns the normal RS from solely nominal images and prevents representational collapse with the use of an ‘anchor’ and stop loss. Anomalies are identified based on their distance to the normal RS.

3 Materials

The baseline cohort from the Osteoarthritis Initiative (OAI) [12,26] was used for this analysis as it is the most commonly used subset in the literature. The OAI is an observational, longitudinal study of 4,796 subjects across 431,000 clinical studies with the goal of better understanding of prevention and treatment of knee osteoarthritis [26]. The images are of size 224×224 , with 5,778 available for training, 826 available for validation and 1,526 available for testing. It was ensured that both knees belonging to a single patient were within the same dataset split to prevent any data leakage. The dataset provides the KL grades and a grading for both the severity of JSN and osteophytes on a scale from zero to three. The grading for JSN and osteophytes are provided for medial and lateral tibiofemoral compartments separately. According to the OARSI scale, OA is diagnosed if any of the following criteria are met; either JSN grade ≥ 2 , sum of osteophyte grades ≥ 2 or grade one JSN in combination with a grade one osteophyte [14,15]. The dataset contained missing values for osteophyte gradings in some cases. As the missing values solely occurred when the KL grades were equal to zero or one and the JSN for both the medial and lateral compartments

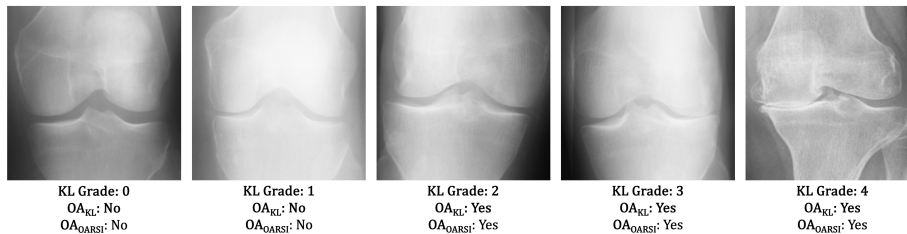


Fig. 1. Examples of X-rays from the training set with for each KL grade. OA_{KL} refers to whether OA was diagnosed based on the KL scale and OA_{OARSI} refers to whether OA was diagnosed based on the OARSI criteria.

had a grade of zero, we labelled these cases as not having OA according to the OARSI scale. Examples of a knee X-ray for each grade are shown in figure 1. Table 1 shows the breakdown of the class balances for each split.

Table 1. The number of X-rays in each dataset split and the number of X-rays that were diagnosed with OA according to the KL system (OA_{KL}) and the OARSI system (OA_{OARSI}).

Split	Grade 0	Grade 1	Grade 2	Grade 3	Grade 4	OA_{KL}	OA_{OARSI}
Train	2286	1046	1516	757	173	2446	2436
Validation	328	153	212	106	27	345	342
Test	639	296	447	223	51	721	706

4 Methods

4.1 Stage 1: Self-Supervised Learning

The purpose of SSL is to learn a representation of healthy X-rays. There are K ensembles trained on a dataset X_N of size N , where X_N is sampled from the training data, X_{train} which consists of solely nominal images of healthy X-rays. In iteration i of training, a data sample $x_i \in X_N$ is paired with a randomly selected data sample $x_j \in X_N$. The original FewSOME implementation relies on ImageNet pretrained weights and an ‘anchor’ for learning compact representations of the normal class where the ground truth label, y is equal to zero for the duration of training. This work extends this method to use SSL where both data samples, x_i and x_j are input into a Stochastic Data Augmentation (SDA) module. The SDA module consists of two sets of transforms, T_{norm} and T_{anom} . The set of transforms T_{norm} are applied only to x_i and they consist of weak, global augmentations that aim to generate additional X-rays whose representation are within the hyper-sphere of the normal RS. T_{norm} consists of the identity function (i.e. no transformation), applying jitter to the image and adjusting the sharpness and brightness. The set of transforms T_{anom} are applied only to x_j and

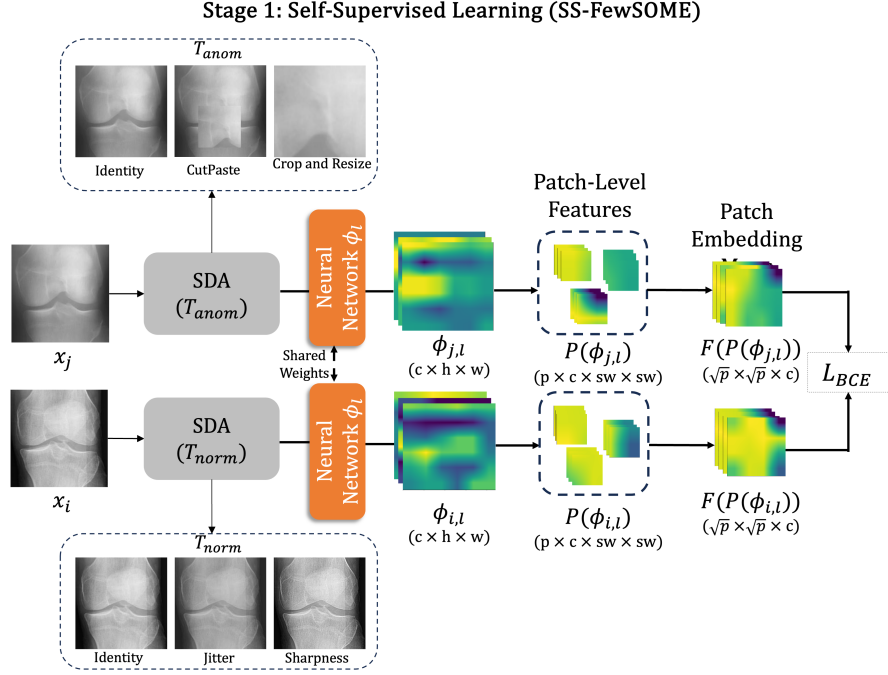


Fig. 2. The figure shows iteration i of training where a data sample $x_i \in X_N$ is paired with a randomly selected data sample $x_j \in X_N$. Following the SDA, both instances are input in tandem into the neural network ϕ_l . The output, denoted as $\phi_{i,l}$ and $\phi_{j,l}$ is converted to patch level features, $P(\phi_{i,l})$ and $P(\phi_{j,l})$. Following average pooling, the tensor is reshaped to create patch embedding maps, $F(P(\phi_{i,l}))$ and $F(P(\phi_{j,l}))$. The patch embedding map, $F(P(\phi_{i,l}))$ consists of p patches at coordinates z, k , where each patch is denoted as $p_{i,z,k}$. The Cosine Distance (CD) is calculated between each patch, $p_{i,z,k}$ and $p_{j,z,k}$ at the same coordinates z, k . The loss is calculated as the Binary Cross Entropy between the CD between patches and each ground truth label, $y_{i,x,k}$

they consist of the identity function and strong augmentations, random cropping followed by resizing and Cutpaste [23]. Section 7.2 presents the results of experiments conducted to choose the optimal performing transforms for T_{anom} .

Following the SDA, the first l layers of a neural network, ϕ , initialised with ImageNET [31] pre-trained weights are used to transform the input space, X_N to the RS, $\phi_l(X_N) \in \mathbb{R}^{c \times h \times w}$, where c is the number of channels, h is the height and w is the width of the extracted feature maps. The later layers are removed as they are biased towards natural image classification. As the size of the training dataset is small, both $\phi_l(x_i)$ and $\phi_l(x_j)$, denoted as $\phi_{i,l}$ and $\phi_{j,l}$, are converted to patch level features, $P(\phi_{i,l})$ and $P(\phi_{j,l})$ using a sliding window of size $sw \times sw$ with $stride = 1$ with resulting dimensions of $p \times c \times sw \times sw$ where p is the number of patches. The patch level features also improve the sensitivity of the model to localised anomalies such as osteophytes. Feature aggregation is performed by average pooling for each patch and the resultant tensor is reshaped

to create patch embedding maps, $F(P(\phi_{i,l}))$ and $F(P(\phi_{j,l})) \in \mathbb{R}^{\sqrt{p} \times \sqrt{p} \times c}$. The patch embedding map, $F(P(\phi_{i,l}))$ consists of p patches at coordinates z, k , where each patch is denoted as $p_{i,k,z}$.

This method exploits that X-rays are spatially similar and therefore, the Cosine Distance, CD is calculated only between patches $p_{i,z,k} \in F(P(\phi_{i,l}))$ and $p_{j,z,k} \in F(P(\phi_{j,l}))$ that have the same coordinates, z, k . The ground truth label $y_{i,z,k} \forall (z, k)$ is equal to zero if the identity transform in the SDA was applied to x_j and $y_{i,z,k} \forall (z, k)$ is equal to one if cropping and resizing was applied. In the case of applying the CutPaste transform, the entire image is not affected and therefore, $y_{i,z,k}$ is equal to one if the receptive field of $p_{j,z,k}$ was affected by the CutPasting and zero otherwise. The CD between each patch, $p_{i,z,k}$ and $p_{j,z,k}$ is calculated as shown in equation 1 and denoted as $\hat{y}_{i,z,k}$. The difference between $\hat{y}_{i,z,k}$ and the ground truth label, $y_{i,z,k}$ are minimised using Binary Cross Entropy during training as shown in equation 2.

$$\hat{y}_{i,z,k} = 1 - \frac{p_{i,z,k} \cdot p_{j,z,k}}{\|p_{i,z,k}\| \|p_{j,z,k}\|} \quad (1)$$

$$\mathcal{L}_{BCE} = -\frac{1}{N \cdot \sqrt{p} \cdot \sqrt{p}} \sum_{i=1}^N \sum_{z=1}^{\sqrt{p}} \sum_{k=1}^{\sqrt{p}} y_{i,z,k} \cdot \log(\hat{y}_{i,z,k}) + (1 - y_{i,z,k}) \cdot \log(1 - \hat{y}_{i,z,k}) \quad (2)$$

4.2 Stage 2: Pseudo Labelling and Denoising with CLIP

Given an unlabelled dataset of X-rays, X_u of size u where $X_u \cap X_N = \emptyset$, the patch embedding map, $F(P(\phi_{u,l}))$ consisting of patches p , for each data sample $x \in X_u$ is obtained. The centre, C_{norm} of the normal RS is then calculated as in equation 3. An anomaly scoring function, S_{SSL} assigns x_u an Anomaly Score (AS) equal to the average CD to the centre C_{norm} , as shown in equation 4.

$$C_{norm} = \frac{1}{N \cdot \sqrt{p} \cdot \sqrt{p}} \sum_{i=1}^N \sum_{z=1}^{\sqrt{p}} \sum_{k=1}^{\sqrt{p}} p_{i,z,k} \quad (3)$$

$$S_{SSL}(x_u) = \frac{1}{\sqrt{p} \cdot \sqrt{p}} \sum_{z=1}^{\sqrt{p}} \sum_{k=1}^{\sqrt{p}} 1 - \frac{p_{u,z,k} \cdot C_{norm}}{\|p_{u,z,k}\| \|C_{norm}\|} \quad (4)$$

Each ensemble K identifies a data instance as an anomaly if the AS is greater than m times the maximum CD between all possible pairs in the training data (denoted as CD_{max}), where $1 \leq m \leq \infty$. Data instances that have been voted as an anomaly across all ensembles are then assumed to be severe OA cases. The model can be retrained on these cases to improve the sensitivity to OA specific anomalies with the newly assigned pseudo label of $y = 1$. However, knee X-rays often contain anomalies unrelated to the OA grade, such as the presence of screws and metal in the X-ray due to knee replacement implants [16]. Using

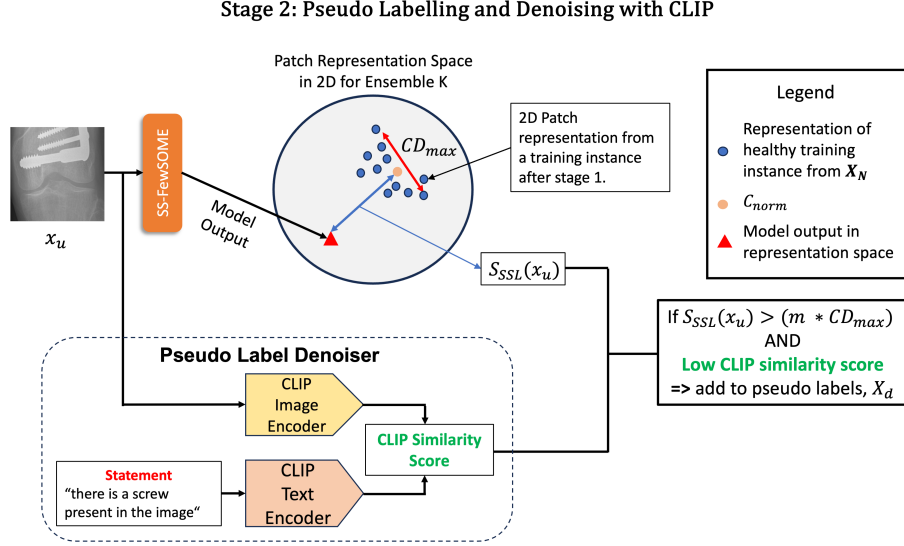


Fig. 3. SS-FewSOME from Stage 1 is used to transform $x_u \in X_u$ to the RS. The AS scoring function, S_{SSL} is then used to pseudo label x_u . The sample x_u is also input into the CLIP image encoder and its similarity is calculated between the image encoding and the text encoding of the compositional statement. If $S_{SSL}(x_u) > (m \times CD_{max})$, x_u is added to the pseudo labels, X_d for Stage 3.

the pre-trained CLIP [28] model with ViT-B/32 Transformer architecture, the similarity between each image and a single compositional statement, ‘there is a screw present in the image’, was obtained. Based on experiments on validation data, an assumption is made that approximately 5% of the labelled training data is affected by the presence of metal in the dataset. Therefore, images with a similarity score greater than the similarity score of the 95th percentile of the training data are considered to be ‘false’ anomalies and they are removed from the pseudo labels, resulting in a dataset X_d of denoised pseudo labels. This stage is conducted only during training. No X-rays are removed during the dataset at test time.

4.3 Stage 3: Dual Centre Representation Learning with FewSOME

Given there are now anomalous psuedo labels available for training, this section proposes Dual Centre Representation Learning (DCRL) with FewSOME. The goal of DCRL is to simultaneously learn two separate RSs for normality and anomalies. DCRL has the same methodology as Stage 1 SSL except the SDA is switched off and the value of y is determined by where x_j is sampled from. For example, in iteration i of training, $x_i \in X_N$ is paired with a randomly selected data sample x_j where $y_i = 0$ if $x_j \in X_N$ and $y_i = 1$ if $x_j \in X_d$. The objective of

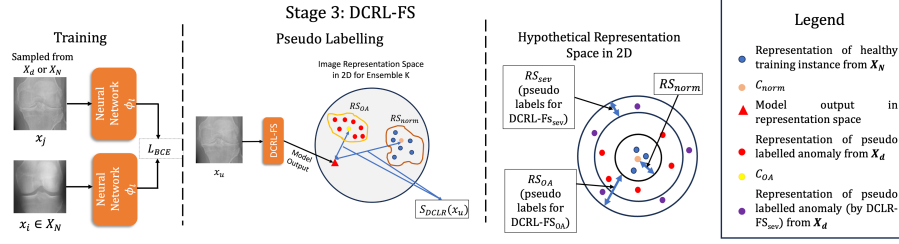


Fig. 4. Stage 3 uses DC to learn two representation spaces, one for normal instances, RS_{norm} and another for anomalies RS_{OA} (or RS_{sev}). The figure also shows a hypothetical representation space demonstrating where the pseudo labels are obtained for $DCRL-FS_{sev}$ and $DCRL-FS_{OA}$.

the training is to transform x_i and x_j to the RS, calculate the CD between the two instances and compare this to the ground truth label y_i .

It was found that the model learns a more robust representation of healthy X-rays when training with pseudo labels of varying OA severity, while it is less robust when exposed to only pseudo labels of severe OA cases (cases with high AS scores output from the model). However, training the model on pseudo labels of more severe OA cases (cases with high AS) results in a highly accurate severe OA detector but a less accurate OA detector. To combat this trade-off, two models are trained, $DCRL-FS_{sev}$ and $DCRL-FS_{OA}$.

$DCRL-FS_{sev}$ is used to learn a RS for healthy cases, RS_{norm} and another for severe OA cases, RS_{sev} . $DCRL-FS_{OA}$ learns a RS for normal OA cases, RS_{norm} and another for all other varying severity OA cases, RS_{OA} . The margin, m controls the level of severity of the pseudo labels. Therefore m is set higher when training $DCRL-FS_{sev}$ and lower when training $DCRL-FS_{OA}$. $DCRL-FS_{OA}$ can be trained iteratively, meaning it can be used to predict additional pseudo labels, which are denoised using the method of Stage 2 and then retrained on the newly assigned pseudo labels.

The models are combined to develop the continuous automated grading system, $DCRL-FS_{comb}$. The CD to the centre C_{norm} of RS_{norm} (obtained from training $DCRL-FS_{sev}$) is denoted as d_1 and the CD to C_{sev} of RS_{sev} is denoted as d_2 . The anomaly scoring function, $S_{DCRL_{sev}}$ is then equal to the difference between the distances d_1 and d_2 as can be seen from equations 5 to 7. Similarly, $S_{DCRL_{OA}}$ is calculated as in equation 8, where d_3 is the CD to the centre C_{norm} of RS_{norm} (obtained from training $DCRL-FS_{OA}$) and d_4 is the CD to the centre C_{OA} of RS_{OA} . The $DCRL-FS_{sev}$ behaves as a severe OA detector, meaning if $S_{DCRL_{sev}}$ is greater than a threshold, t , x_u is assigned a score of $1 + S_{DCRL_{sev}}(x_u)$, as $0 \leq S_{DCRL_{OA}}(x_u) \leq 1$. Otherwise it is equal to $S_{DCRL_{OA}}(x_u)$, as shown in equation 9.

$$d_1 = 1 - \frac{DCRL-FS_{sev}(x_u) \cdot C_{norm}}{\|DCRL-FS_{sev}(x_u)\| \|C_{norm}\|} \quad (5)$$

$$d_2 = 1 - \frac{DCRL-FS_{sev}(x_u) \cdot C_{sev}}{\|DCRL-FS_{sev}(x_u)\| \|C_{sev}\|} \quad (6)$$

$$S_{DCRL_{sev}} = \|d_1 - d_2\| \quad (7)$$

$$S_{DCRL_{OA}} = \|d_3 - d_4\| \quad (8)$$

$$S_{DCRL_{comb}}(x_u) = \begin{cases} 1 + S_{DCRL_{sev}}(x_u), & \text{if } S_{DCRL_{sev}}(x_u) > t \\ S_{DCRL_{OA}}(x_u), & \text{otherwise} \end{cases} \quad (9)$$

5 Implementation Details

The hyper-parameters including the model backbones were selected based on the model’s performance on the validation set. The models were trained with a batch size of one, a learning rate of $1e - 06$, Adam optimiser [21] and weight decay of 0.1.

5.1 Stage 1

The size of the training set for each ensemble, was set to 30 ($N = 30$) as per the original FewSOME [7] implementation. The size of the training data, X_{train} (the data where N is sampled from for each ensemble) was set to 150 and a total of $K = 10$ ensembles were trained. Section 7.3 presents an analysis to motivate the selection of a training set size of 150 examples. The first five layers of an AlexNET [22] was employed as the model backbone. Training was halted once the training loss began to plateau.

5.2 Stage 3_{iter1}

As X-rays with psuedo labels are now available for training in stage 3, the larger VGG-16 [33] is employed. The margin, m was set to 1.184 to obtain the pseudo labels for DCRL-FS_{OA} as this resulted in a balanced number of normal instances and anomalous instances (30 pseudo labels). Based on experiments on validation data, the margin m was set to 3.122 to obtain the pseudo labels to train DCRL-FS_{sev}. The threshold t for combining the models was set to the AS of the 95% percentile of the training data as output by DCRL-FS_{sev}. The training is halted when the CD between the normal centre, C_{norm} and anomalous centres C_{OA} (when training DCRL-FS_{OA}) or C_{sev} (when training DCRL-FS_{sev}) begins to plateau. Section 7.4 presents an analysis of the effects of this early stopping technique.

5.3 Stage 3_{iterfinal}

As previously mentioned, DCRL-FS_{OA} can be trained iteratively. In the second iteration, the number of pseudo labels was equal to 263 for DCRL_{OA} (with $m = 1.184$ as before). To avoid a large class imbalance, the number of training instances for each ensemble was increased from 30 to 150 (all available labelled training data). The model was not trained for further iterations as it reached optimal performance.

5.4 Competing Methods

Stage 1 SS-FewSOME’s performance is compared to competing methods, DeepSVDD [30], SOTA AD technique PatchCore [29] and few shot AD technique FewSOME [7]. As the original implementation of DeepSVDD is compatible with small images of 32×32 , the images are downsampled to 128×128 and the architecture is upscaled by increasing the number of kernels. Competing methods were trained on 150 samples of normal X-rays as was SS-FewSOME.

Stage 3 Final Iteration The final iteration of the model is compared to DDAD [11], a SOTA model in medical AD, as it trains on both labelled and unlabelled data. DDAD is trained on 150 labelled healthy knee X-rays and 5,628 unlabelled X-rays. This is the most similar set-up to the stage 3 of the proposed method as it trains on 150 labelled healthy knee X-rays and there were 5,628 unlabelled X-rays available for pseudo labelling.

6 Results

The methodology is assessed based on its ability to diagnose OA according to the KL scale (grades ≥ 2) and the OARSI scale. Table 2 reports the Area Under the Receiver Operator Curve (AUC) in % for both tasks, denoted as AUC_{KL} and AUC_O . The Spearman Rank Correlation Coefficient (SRC) between the model output and the KL grade is also reported as SRC_{KL} . Finally, to ensure that the model can identify severe OA cases to a high degree of accuracy, the table reports the performance of detecting cases with KL grades > 3 as $AUC_{KL_{g>3}}$.

6.1 Stage 1

Each method had 150 training instances available for training. The proposed SS-FewSOME significantly outperforms competing methods and it shows substantial performance improvement on the original FewSOME implementation, increasing the AUC_{KL} from 58.3% to 72.9%. The results also show that integrating the patches method into the model has resulted in a performance improvement, increasing SRC_{KL} from 0.315 to 0.432.

Table 2. AUC in % with one standard deviation over five seeds. The standard deviations of ensemble methods are the standard deviations of performance between each ensemble. SS-FewSOME abbreviated to SS-FS. The * highlights the two models that were combined for DCRL-FS_{comb} in stage 3_{iter1}

Method	Stage	Patches	AUC _{KL}	AUC _O	AUC _{KL_g>3}	SRC _{KL}
DeepSVDD [30]	1	-	54.8 ± 1.0	55.8 ± 0.9	62.3 ± 2.2	0.097 ± 0.0
Patchcore [29]	1	-	64.6 ± 0.6	65.7 ± 0.5	89.1 ± 0.6	0.270 ± 0.0
FewSOME [7]	1	✓	58.3 ± 0.2	54.8 ± 3.4	67.8 ± 0.7	0.144 ± 0.5
SS-FS	1	×	66.8 ± 0.7	66.8 ± 0.9	85.4 ± 0.4	0.315 ± 0.0
SS-FS	1	✓	72.9 ± 1.0	73.7 ± 1.1	89.4 ± 1.9	0.432 ± 0.0
DCRL-FS _{OA} *	3 _{iter1}	×	78.6 ± 1.4	79.5 ± 1.2	95.2 ± 1.5	0.539 ± 0.0
DCRL-FS _{sev} *	3	×	76.9 ± 1.1	77.3 ± 1.1	97.6 ± 0.4	0.491 ± 0.0
DCRL-FS _{comb} **	3 _{iter1}	×	78.6 ± 1.4	79.5 ± 1.2	97.2 ± 0.4	0.541 ± 0.0
DCRL-FS _{OA}	3 _{iterfinal}	×	81.0 ± 0.2	81.6 ± 0.1	95.7 ± 0.4	0.580 ± 0.0
DCRL-FS _{comb}	3 _{iterfinal}	×	81.0 ± 1.4	81.6 ± 1.2	97.6 ± 0.4	0.583 ± 0.0
DDAD [11]	-	-	56.7 ± 0.6	57.2 ± 0.6	69.7 ± 0.9	0.130 ± 0.0

6.2 Stage 3_{iter1}

The trade-off between OA detection and severe OA detection accuracy can be evidently seen from the results of DCRL-FS_{OA} (stage 3_{iter1}) and DCRL-FS_{sev}, with the former outperforming DCRL-FS_{sev} in terms of OA detection but underperforming in terms of severe OA detection. However, the combined model DCRL-FS_{comb} (stage 3_{iter1}) combines both aspects of the models to accurately detect OA, severe OA and correlate with the KL grades with an SRC of 0.541. Figure 5 shows the distance of each data instance in the test set from C_{norm} at stage 1 and stage 3_{iter1}. Separation between classes can be evidently seen at

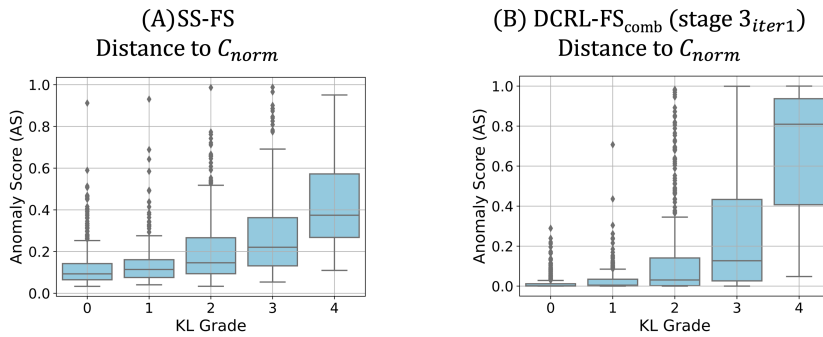


Fig. 5. Boxplot of distances of each instance from the test set to C_{norm} in RS at (A) stage 1, SS-FewSOME (SS-FS) and (B) stage 3_{iter1}



Fig. 6. Examples that were assigned the highest anomaly scores by DCRL-FS_{OA} (stage 3_{iter1}). These examples are severe OA cases and display OA characteristics such as JSN and osteophytes.

stage 1 and furthermore at stage 3_{iter1}. Figure 6 presents the most anomalous examples as output by DCRL-FS_{comb} (stage 3_{iter1}). The common symptoms of OA are apparent such as JSN and the presence of osteophytes.

6.3 Stage 3_{iterfinal}

The final iteration achieved an SRC of 0.583, a promising result given the inter-rater reliability of human experts was reported to be as low as 0.51 in some cases [37]. The proposed methodology outperforms the competing method DDAD [11] by margins of up to 24%, which was trained on 150 labelled healthy knee X-rays and 5,628 unlabelled X-rays. Notably, the proposed work outperforms the previous OA automated continuous system that reports an SRC of 0.524 (averaged across classes), having trained on 10,012 labelled images [24]. Additionally, a paired student t-test showed that the difference between the mean model output for each KL grade was statistically significant at the 5% significance level.

7 Further Analysis

7.1 CLIP Ablation

To demonstrate the effectiveness of denoising the pseudo labels with CLIP, DCRL-FS_{OA} at stage 3_{iter1} was also trained without denoising. This resulted in a performance degradation as can be seen from table 3. Figure 7 presents examples of false anomalies that were denoised by CLIP.

Table 3. AUC in % with one standard deviation over five seeds.

Method	Stage	AUC _{KL}	AUC _O	AUC _{KL_g>3}	SRC _{KL}
DCRL-FS _{comb}	3 _{iter1}	78.6 ± 1.4	79.5 ± 1.2	97.2 ± 0.4	0.541 ± 0.0
DCRL-FS _{OA} (No CLIP)	3 _{iter1}	75.6 ± 2.0	76.3 ± 1.9	93.6 ± 1.1	0.485 ± 0.0

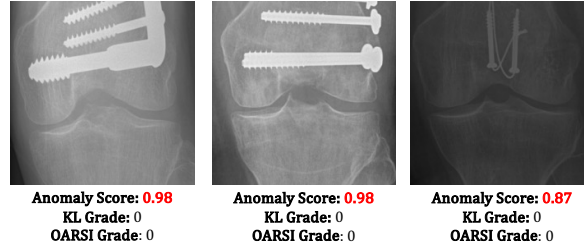


Fig. 7. Samples from X_u that were assigned high anomaly scores from SS-FewSOME. These examples were then denoised using the CLIP model and they were removed from the pseudo labels for Stage 3, DCRL training.

7.2 Analysis of Transforms for T_{anom}

The following transforms were assessed for inclusion in T_{anom} : posterising which limits the number of tones and colours in the image, random rotate, random crop and CutPaste [23] which takes a segment of the image and pastes it elsewhere on the image. Table 4 presents the results of each transform on the validation set. CutPaste outperforms the other transforms by a substantial margin. As a combination of cropping and CutPaste resulted in the optimal performance, they were selected for the final model. Examples of the transforms are shown in figure 8.

Table 4. The table shows the performance of each transform from T_{anom} on the validation set.

Method	AUC_{KL}	AUC_O	$AUC_{KL_g \geq 3}$	SR_{KL}
Posterise _{2bits}	59.8 ± 1.5	60.2 ± 1.7	67.6 ± 2.1	0.174 ± 0.0
Rotate _{>90°, <270°}	58.4 ± 0.8	58.0 ± 0.7	77.2 ± 3.4	0.140 ± 0.0
Crop	59.6 ± 1.0	59.6 ± 1.0	76.7 ± 1.5	0.177 ± 0.0
CutPaste	72.1 ± 1.1	72.4 ± 1.3	87.1 ± 2.4	0.388 ± 0.0
Crop + CutPaste	73.3 ± 0.7	72.9 ± 0.7	92.9 ± 1.0	0.400 ± 0.0

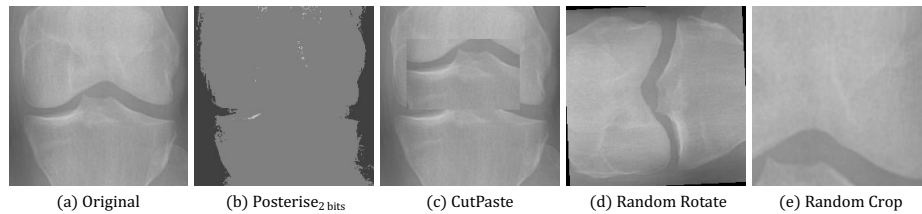


Fig. 8. Examples of transforms that were assessed for inclusion in T_{anom} for Stage 1 SSL.

7.3 Training Set Size Analysis

Figure 9 shows the model performance for each metric for varying sizes of X_{train} . As SS-FewSOME in stage 1 trains on $N = 30$, each training set size represents an ensemble of models training on $N = 30$. For example, a training set size of 60 is two ensembles training on $N = 30$. It can be seen from the figure that there a plateau in performance begins between 90 to 150 training instances. Therefore, the experiments were conducted training on 150 labelled instances. The figure also demonstrates how SS-FewSOME can achieve optimal performance on small training set sizes of as low as 90 examples.

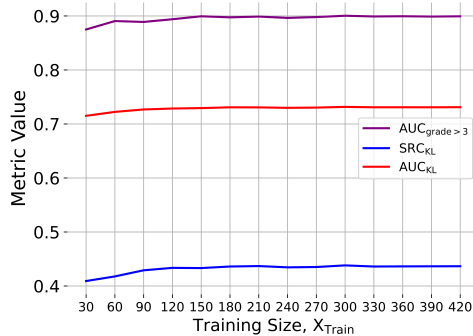


Fig. 9. The average result for each metric, on the test set for stage 1 for varying training set sizes, X_{train} .

7.4 Analysis of Early Stopping

In stage 3, training is halted when the CD between the centres, C_{norm} and C_{OA} begins to plateau. Figure 10 (A) shows the average value for each metric (AUC_{KL} , AUC_{OARSI} , $AUC_{grade > 3}$ and SRC_{KL}) over ten seeds for each epoch on the test set for DCRL-FS_{OA} at stage 3_{iter1}. The black vertical line shows where early stopping occurred on average. It can be seen from the figure that there is no further performance increase after early stopping and overfitting has not occurred by the time of early stopping. Figure 10 (B) shows the CD between centres C_{norm} and C_{OA} at each epoch.

8 Conclusion

This work has demonstrated the potential for a continuous disease severity grading system, which holds promise for substantial clinical impact by eliminating subjectivity and enabling the assessment of disease severity at any stage along

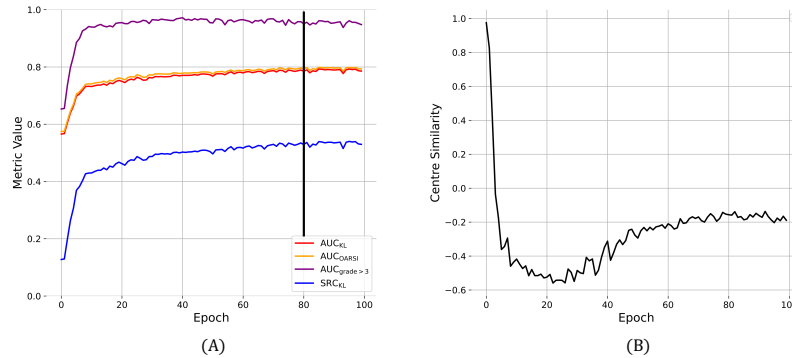


Fig. 10. (A) shows the average value for each metric (AUC_{KL} , AUC_{OARSI} , $AUC_{grade>3}$ and SRC_{KL}) over ten seeds for each epoch on the test set for Stage 3_{iter1} . The black vertical line shows where the average early stopping occurred over the ten seeds. Early stopping is based on the plateau of the centre similarities as seen in (B).

a continuum, rather than predefined discrete categories. This method is particularly useful for capturing subtle variations and changes over time, providing a more detailed and dynamic understanding of the condition’s progression, ultimately resulting in improved patient care. The analysis showed that the proposed method outperforms existing methods by significant margins and can achieve human level performance whilst training on few labels, thus eliminating the requirement for large annotated databases.

Acknowledgements

This work was funded by Science Foundation Ireland through the SFI Centre for Research Training in Machine Learning (Grant No. 18/CRT/6183). This work is supported by the Insight Centre for Data Analytics under Grant Number SFI/12/RC/2289 P2.

References

1. Abedin, J., Antony, J., McGuinness, K., Moran, K., O’Connor, N.E., Rebolz-Schuhmann, D., Newell, J.: Predicting knee osteoarthritis severity: comparative modeling based on patient’s data and plain x-ray images. vol. 9, pp. 392–408 (2019)
2. Altman, R.D., Gold, G.: Atlas of individual radiographic features in osteoarthritis, revised. *Osteoarthritis and cartilage* **15**, A1–A56 (2007)
3. Altman, R.D., Hochberg, M., Murphy Jr, W., Wolfe, F., Lequesne, M.: Atlas of individual radiographic features in osteoarthritis. *Osteoarthritis and cartilage* **3**, 3–70 (1995)

4. Antony, J., McGuinness, K., Moran, K., O'Connor, N.E.: Automatic detection of knee joints and quantification of knee osteoarthritis severity using convolutional neural networks. In: Machine Learning and Data Mining in Pattern Recognition: 13th International Conference, MLDM 2017, New York, NY, USA, July 15-20, 2017, Proceedings 13. pp. 376–390. Springer (2017)
5. Bany Muhammad, M., Yeasin, M.: Interpretable and parameter optimized ensemble model for knee osteoarthritis assessment using radiographs. *Scientific Reports* **11**(1), 14348 (2021)
6. Baur, C., Graf, R., Wiestler, B., Albarqouni, S., Navab, N.: Steganomaly: Inhibiting cyclegan steganography for unsupervised anomaly detection in brain mri. In: International Conference on Medical Image Computing and Computer-Assisted Intervention. pp. 718–727. Springer (2020)
7. Belton, N., Hagos, M.T., Lawlor, A., Curran, K.M.: Fewsome: One-class few shot anomaly detection with siamese networks. In: Proceedings of the IEEE/CVF Conference on Computer Vision and Pattern Recognition Workshops. pp. 2977–2986 (2023)
8. Belton, N., Hagos, M.T., Lawlor, A., Curran, K.M.: Towards a unified approach for unsupervised brain mri motion artefact detection with few shot anomaly detection. *Computerized Medical Imaging and Graphics* **115**, 102391 (2024)
9. Belton, N., Lawlor, A., Curran, K.M.: Semi-supervised siamese network for identifying bad data in medical imaging datasets [short paper presentation]. *Medical Imaging with Deep Learning (MIDL)* (2021), <https://openreview.net/pdf?id=0bpkIn63sNG>
10. Bozorgtabar, B., Mahapatra, D., Vray, G., Thiran, J.P.: Salad: Self-supervised aggregation learning for anomaly detection on x-rays. In: Medical Image Computing and Computer Assisted Intervention–MICCAI 2020: 23rd International Conference, Lima, Peru, October 4–8, 2020, Proceedings, Part I 23. pp. 468–478. Springer (2020)
11. Cai, Y., Chen, H., Yang, X., Zhou, Y., Cheng, K.T.: Dual-distribution discrepancy with self-supervised refinement for anomaly detection in medical images. *Medical Image Analysis* **86**, 102794 (2023)
12. Chen, P.: Knee osteoarthritis severity grading dataset. *Mendeley Data* **1** (2018)
13. Chen, P., Gao, L., Shi, X., Allen, K., Yang, L.: Fully automatic knee osteoarthritis severity grading using deep neural networks with a novel ordinal loss. *Computerized Medical Imaging and Graphics* **75**, 84–92 (2019)
14. Culvenor, A.G., Engen, C.N., Øiestad, B.E., Engebretsen, L., Risberg, M.A.: Defining the presence of radiographic knee osteoarthritis: a comparison between the kellgren and lawrence system and oarsi atlas criteria. *Knee Surgery, Sports Traumatology, Arthroscopy* **23**, 3532–3539 (2015)
15. Culvenor, A.G., Lai, C.C., Gabbe, B.J., Makdissi, M., Collins, N.J., Vicenzino, B., Morris, H.G., Crossley, K.M.: Patellofemoral osteoarthritis is prevalent and associated with worse symptoms and function after hamstring tendon autograft acl reconstruction. *British journal of sports medicine* (2013)
16. Cyteval, C.: Imaging of knee implants and related complications. *Diagnostic and interventional imaging* **97**(7-8), 809–821 (2016)
17. Farooq, M.U., Ullah, Z., Khan, A., Gwak, J.: Dc-aae: Dual channel adversarial autoencoder with multitask learning for kl-grade classification in knee radiographs. *Computers in Biology and Medicine* p. 107570 (2023)
18. Jain, R.K., Sharma, P.K., Gaj, S., Sur, A., Ghosh, P.: Knee osteoarthritis severity prediction using an attentive multi-scale deep convolutional neural network. *arXiv preprint arXiv:2106.14292* (2021)

19. Jeong, J., Zou, Y., Kim, T., Zhang, D., Ravichandran, A., Dabeer, O.: Winclip: Zero-/few-shot anomaly classification and segmentation. In: Proceedings of the IEEE/CVF Conference on Computer Vision and Pattern Recognition. pp. 19606–19616 (2023)
20. Kellgren, J.H., Lawrence, J.: Radiological assessment of osteo-arthrosis. *Annals of the rheumatic diseases* **16**(4), 494 (1957)
21. Kingma, D.P., Ba, J.: Adam: A method for stochastic optimization. arXiv preprint arXiv:1412.6980 (2014)
22. Krizhevsky, A., Sutskever, I., Hinton, G.E.: Imagenet classification with deep convolutional neural networks. *Advances in neural information processing systems* **25** (2012)
23. Li, C.L., Sohn, K., Yoon, J., Pfister, T.: Cutpaste: Self-supervised learning for anomaly detection and localization. In: Proceedings of the IEEE/CVF Conference on Computer Vision and Pattern Recognition. pp. 9664–9674 (2021)
24. Li, M.D., Chang, K., Bearce, B., Chang, C.Y., Huang, A.J., Campbell, J.P., Brown, J.M., Singh, P., Hoebel, K.V., Erdoğan, D., et al.: Siamese neural networks for continuous disease severity evaluation and change detection in medical imaging. *NPJ digital medicine* **3**(1), 48 (2020)
25. M, G.K., Goswami, A.D.: Automatic classification of the severity of knee osteoarthritis using enhanced image sharpening and cnn. *Applied Sciences* **13**(3) (2023). <https://doi.org/10.3390/app13031658>, <https://www.mdpi.com/2076-3417/13/3/1658>
26. Nevitt, M., Felson, D., Lester, G.: The osteoarthritis initiative. *Protocol for the cohort study* **1** (2006)
27. Olsson, S., Akbarian, E., Lind, A., Razavian, A.S., Gordon, M.: Automating classification of osteoarthritis according to kellgren-lawrence in the knee using deep learning in an unfiltered adult population. *BMC musculoskeletal disorders* **22**(1), 1–8 (2021)
28. Radford, A., Kim, J.W., Hallacy, C., Ramesh, A., Goh, G., Agarwal, S., Sastry, G., Askell, A., Mishkin, P., Clark, J., et al.: Learning transferable visual models from natural language supervision. In: International conference on machine learning. pp. 8748–8763. PMLR (2021)
29. Roth, K., Pemula, L., Zepeda, J., Schölkopf, B., Brox, T., Gehler, P.: Towards total recall in industrial anomaly detection. In: Proceedings of the IEEE/CVF Conference on Computer Vision and Pattern Recognition. pp. 14318–14328 (2022)
30. Ruff, L., Vandermeulen, R., Goernitz, N., Deecke, L., Siddiqui, S.A., Binder, A., Müller, E., Kloft, M.: Deep one-class classification. In: ICML. pp. 4393–4402. PMLR (2018)
31. Russakovsky, O., Deng, J., Su, H., Krause, J., Satheesh, S., Ma, S., Huang, Z., Karpathy, A., Khosla, A., Bernstein, M., et al.: Imagenet large scale visual recognition challenge. *International journal of computer vision* **115**, 211–252 (2015)
32. Saini, D., Khosla, A., Chand, T., Chouhan, D.K., Prakash, M.: Automated knee osteoarthritis severity classification using three-stage preprocessing method and vgg16 architecture. *International Journal of Imaging Systems and Technology* (2023)
33. Simonyan, K., Zisserman, A.: Very deep convolutional networks for large-scale image recognition. arXiv preprint arXiv:1409.1556 (2014)
34. Tiulpin, A., Thevenot, J., Rahtu, E., Lehenkari, P., Saarakkala, S.: Automatic knee osteoarthritis diagnosis from plain radiographs: a deep learning-based approach. *Scientific reports* **8**(1), 1727 (2018)

35. Vos, T., Flaxman, A.D., Naghavi, M., Lozano, R., Michaud, C., Ezzati, M., Shibuya, K., Salomon, J.A., Abdalla, S., Aboyans, V., et al.: Years lived with disability (ylds) for 1160 sequelae of 289 diseases and injuries 1990–2010: a systematic analysis for the global burden of disease study 2010. *The lancet* **380**(9859), 2163–2196 (2012)
36. Wahyuningrum, R.T., Anifah, L., Purnama, I.K.E., Purnomo, M.H.: A new approach to classify knee osteoarthritis severity from radiographic images based on cnn-lstm method. In: 2019 IEEE 10th International Conference on Awareness Science and Technology (iCAST). pp. 1–6. IEEE (2019)
37. Wright, R.W., Ross, J.R., Haas, A.K., Huston, L.J., Garofoli, E.A., Harris, D., Patel, K., Pearson, D., Schutzman, J., Tarabichi, M., et al.: Osteoarthritis classification scales: interobserver reliability and arthroscopic correlation. *The Journal of bone and joint surgery. American volume* **96**(14), 1145 (2014)
38. Yoon, J.S., Yon, C.J., Lee, D., Lee, J.J., Kang, C.H., Kang, S.B., Lee, N.K., Chang, C.B.: Assessment of a novel deep learning-based software developed for automatic feature extraction and grading of radiographic knee osteoarthritis. *BMC musculoskeletal disorders* **24**(1), 869 (2023)
39. Zavrtnik, V., Kristan, M., Skočaj, D.: Reconstruction by inpainting for visual anomaly detection. *Pattern Recognition* **112**, 107706 (2021)
40. Zhou, K., Li, J., Luo, W., Li, Z., Yang, J., Fu, H., Cheng, J., Liu, J., Gao, S.: Proxy-bridged image reconstruction network for anomaly detection in medical images. *IEEE Transactions on Medical Imaging* **41**(3), 582–594 (2021)